A peptide of a type I toxin-antitoxin system induces *Helicobacter pylori* morphological transformation from spiral-shape to coccoids

Short title: *H. pylori* shape conversion induced by a TA toxin

Lamya El Mortaji [1], Stéphanie Marsin [2+], Aline Rifflet [3,4], Ivo G. Boneca [3,4], J. Pablo Radicella [2], Gérard Péhau-Arnaudet [5] and Hilde De Reuse [1] *

[1] Institut Pasteur, Département de Microbiologie, Unité Pathogenèse de *Helicobacter*, ERL CNRS 6002, 28 rue du Dr Roux 75724 PARIS Cedex 15 FRANCE.

[2] CEA, Institute of Molecular and Cellular Radiobiology, Institut François Jacob, INSERM UMR967, Universités Paris Diderot et Paris Sud, Fontenay-aux-Roses, France.

+ Current affiliation: I2BC/UMR 9198 CNRS- CEA -Université Paris Sud, Bat. 430, Orsay, FRANCE.

[3] Institut Pasteur, Département de Microbiologie, Unité Biologie et Génétique de la Paroi Bactérienne, 75724 PARIS, FRANCE.

[4] INSERM, Equipe Avenir, 75015 Paris, France

[5] Institut Pasteur, Ultrastructural BioImaging (*UTechS* UBI) /UMR CNRS 3528, PARIS, FRANCE.

* -Corresponding author: Hilde De Reuse (hdereuse@pasteur.fr)

Institut Pasteur, Unité Pathogenèse de *Helicobacter*

28, rue du Docteur Roux

75724 PARIS Cedex 15 FRANCE

Tel : +33 1 40 61 36 41

Summary

Toxin-antitoxin systems are found in many bacterial chromosomes and plasmids with roles ranging from plasmid stabilization to biofilm formation and persistence. In these systems, the expression/activity of the toxin is counteracted by an antitoxin, which in type I systems is an antisense-RNA. While the regulatory mechanisms of these systems are mostly well-defined, the toxins' biological activity and expression conditions are less understood. Here, these questions were investigated with a type I toxin-antitoxin system (AapA1-IsoA1) expressed from the chromosome of the major human pathogen *Helicobacter pylori*. We show that expression of the AapA1 toxin in *H. pylori* causes growth arrest associated with massive morphological transformation from spiral-shaped bacteria to round coccoid cells. Coccoids are observed in patients and during *in vitro* growth as a response to different conditions such as oxidative stress. The AapA1 toxin, first molecular effector of coccoids to be identified, targets *H. pylori* inner membrane without disruption, as visualized by Cryo-EM. The peptidoglycan composition of coccoids is modified as compared to spiral bacteria. No major changes in membrane potential or ATP concentration result from AapA1 expression, suggesting coccoid viability. Using single-cell live microscopy, we observed that shape conversion is associated with cell division interference. Oxidative stress represses antitoxin promoter activity and enhances processing of its transcript leading to an imbalanced ratio in favor of AapA1 toxin expression.

Our data are in favor of viable coccoids with characteristics of dormant bacteria that might be important in *H. pylori* infections refractory to treatment.

Significance Statement

Helicobacter pylori, a gastric pathogen responsible for 800,000 deaths in the world every year, is encountered, both *in vitro* and in patients, as spiral-shaped bacteria and as round cells named coccoids. We discovered that the toxin from a chromosomal type I toxin-antitoxin system is targeting *H. pylori* membrane and acting as an effector of the morphological conversion of *H. pylori* to coccoids. We showed that these round cells maintain their membrane integrity and metabolism, strongly suggesting that they are viable dormant bacteria. Oxidative stress was identified as a signal inducing toxin expression. Our findings reveal new insights into a form of dormancy of this bacterium that might be associated with *H. pylori* infections refractory to treatment.

Introduction

Toxin-antitoxin (TA) systems are small genetic elements that are widely distributed on bacterial mobile genetic elements and among archaeal and bacterial genomes, often in multiple copies (1-3). They code for a small stable toxic protein, designated toxin, whose action or expression is counteracted by an unstable antitoxin molecule that can either be an RNA or a protein (3, 4). Under conditions in which the toxins can act, they target essential cellular processes or components (transcription, DNA replication, translation, cell wall or membrane) resulting in growth arrest or cell death (3, 4). The molecular mechanism of the toxins' activities and their regulation are often known in detail while the biological function remains elusive. TA systems take part in plasmid maintenance and protection from phage infection. Less is known on the biological functions and targets of the chromosomally encoded TA systems. Some are important for bacterial survival in their mammalian host (5) or biofilm formation (6). There is accumulating evidence that upon stress conditions, some TA systems play a role in the switch of actively growing bacteria to persisters or dormant cells (7, 8). Persister bacteria constitute a subpopulation that is metabolically active but slow-growing and highly tolerant to antibiotics and stress conditions (9). Persistence is considered as an important cause of recalcitrance of chronic bacterial infections to therapy. However, stress-induced activation of TA-encoded toxins does not necessarily cause persister formation (10) and it was more generally found that decreased intracellular ATP concentration is a landmark of persister formation (11).

In the present work, we explored the role of TA systems in *Helicobacter pylori*, a bacterium that colonizes the stomach of half of the human population worldwide and causes the development of gastritis. In some cases, gastritis evolves into peptic ulcer disease or gastric carcinoma that causes about 800,000 deaths in the world every year (12, 13). This microaerophilic bacterium is unique in its capacity to persistently colonize the stomach despite its extreme acidity and intense immune response (13). The molecular mechanisms at

the origin of this exceptional adaptation capacity of *H. pylori* remain only partially understood and their elucidation is crucial to understand its virulence and to improve its eradication in patients with recurrent peptic ulcer disease. *H. pylori* is a Gram-negative bacterium with a helical shape. Upon stress conditions (antibiotics, aerobic growth) or prolonged culture, the shape of *H. pylori* progressively evolves into a U-shape followed by a spherical form designated coccoid (14, 15). *H. pylori* coccoids are non-culturable bacteria proposed to be dormant forms (15). Recently, dormant non culturable cells were associated wit a deeper state of dormancy when compared to persister cells (16)

Coccoids were observed in human gastric biopsies and like spirals adhere to gastric epithelial cells. Despite numerous reports on coccoid forms of *H. pylori*, no cellular effector of this conversion has been reported so far.

In type I TAs, the antitoxin is a small regulatory RNA inhibiting the synthesis of the toxin by base pairing the toxin-encoding mRNA (3, 4, 17, 18). Four families (A-B-C-D) of conserved type I TA systems are expressed from the chromosome of *H. pylori*, only the A family was studied as it is highly expressed and conserved among *H. pylori* strains (19, 20). For the A1 TA system, the detailed mechanism by which transcription of the IsoA1 antitoxin RNA impairs AapA1 toxin synthesis by base-pairing with its primary transcript, ensuring both translation inhibition of the AapA1 active message and leading to rapid degradation of the duplex by RNase III has been recently published (20). The *H. pylori* type I toxins are typically small hydrophobic peptides of 30-40 amino acids predicted to form alpha-helices. No clues on the mode of action or the physiological role of these systems have been reported.

Here we show that the AapA1 toxin induces a rapid and massive morphological transformation of *H. pylori* from spirals to coccoids by targeting the inner membrane and interfering with cell division, and that oxidative stress triggers imbalanced expression of the TA components in favor of toxin production.

Results

The AapA1 toxic peptide, expressed by the AapA1/IsoA1 TA system, triggers rapid transformation of *H. pylori* into coccoids

Recently, the study of the AapA1/IsoA1 TA system of *H. pylori* (**Fig. 1A**) showed that expression of the AapA1 toxin (a 30 amino acids-long hydrophobic peptide) leads to bacterial growth arrest (20). Given the genetic organization of the type I AapA1/IsoA1 locus in B128 strain, we decided to investigate the mechanism underlying the activity of AapA1 by using a strain in which AapA1 is under the control of an inducible promoter. We thus transformed *H. pylori* strain B128 deleted of the AapA1/IsoA1 locus with each of the three plasmids constructed by Arnion *et al.* (20) (**Fig. 1A**). The first, pA1-IsoA1, derived of the pILL2157 vector (21) contains a functional TA locus in which the AapA1 gene is under the control of an IPTG inducible promoter (20). In plasmid pA1, derived from this first construct, the antitoxin IsoA1 promoter has been inactivated by point mutations that do not interfere with transcription or translation of the AapA1 ORF (20). Derived from this second construct, plasmid pA1* contains an additional mutation that inactivates the start codon of the AapA1 peptide (20). Under our experimental conditions, we observed, in agreement with data of (20), that addition of IPTG did not significantly influence the growth rate of strains harboring pA1-IsoA1 or pA1*. In contrast, addition of the inducer causes a rapid and immediate growth arrest of *H. pylori* with pA1 indicating a toxic effect of AapA1 expression (**Fig. 1B**). The growth arrest was accompanied by loss of culturability of more than 10^4-fold 8h after induction.

In parallel to growth, we investigated the consequences of AapA1 expression on *H. pylori* morphology. Samples from bacterial cultures with these plasmids were grown in the presence or absence of IPTG, stained with a membrane-specific dye (TMA-DPH) and analyzed by fluorescence microscopy at different time points (**Fig. 1C**). *H. pylori* cells expressing the wild-type AapA1/IsoA1 locus (pA1-IsoA1) or the pA* mutated locus present a classical helical rod shape phenotype upon IPTG exposure (**Fig. 1C**). Under the same conditions, cells

carrying the pA1 plasmid, and thus expressing the AapA1 toxin exhibit a rapid and dramatic morphological conversion to spherical cells also known as coccoid forms. Eight hours after IPTG-induction, some bacteria containing pA1-IsoA1 start to convert to coccoids, this is probably due to accumulation of the AapA1 toxin under these conditions. No bacterial lysis was detected even at 24h post-induction. With strains carrying the pA1* plasmid, coccoids were only observed after 48h of culture, similarly to the control wild type strain containing an empty plasmid. These data show for the first time that the AapA1 toxin induces a fast conversion of *H. pylori* cells from spiral-shaped to coccoid forms.

Inner membrane targeting by the AapA1 toxin

To investigate the mode of action of the AapA1 toxin, we first analyzed its subcellular localization in *H. pylori* using three reporter strains. Two constructs corresponded to C-terminal fusions of the toxin with a SPA-tag (pA1-SPA) (20) or with GFP (pA1-GFP) expressed from the IPTG-inducible promoter of vector pILL2157 (21) (**Fig. S1**). These plasmids were introduced into *H. pylori* strain B128 deleted of the chromosomal AapA1/IsoA1 module. After IPTG induction none of these fusions affected *H. pylori* growth indicating that a C-terminal fusion prevents the toxicity of the toxin. Attempts to construct N-terminal tagged-AapA1 were unsuccessful. In addition, a B128 derivative expressing a chromosomal AapA1-GFP fusion under control of its native promoter was constructed (**Fig. S1**).

Cellular fractionation was then performed on the three strains, and the subcellular localization of the fused toxins was analyzed by immunoblotting. **Figure 2A** shows that upon induction by IPTG, the large majority of the AapA1-SPA is present at the inner membrane of *H. pylori* with no peptide detected in the culture medium. Identical results were obtained with the A1-GFP fusion expressed either from the inducible plasmid or the chromosome (**Fig. S2**). Fluorescence microscopy of live bacteria after induction of the AapA1-GFP fusion revealed a

165 weak patchy pattern in the periphery of the cell (**Fig. 2B**), different from a GFP-alone control
166 cell (**Fig. S2**), and compatible with membrane localization. This observation was confirmed
167 by measuring the overlap of the fluorescence intensity profiles of the toxin and TMA-PH
168 measured perpendicular to the length axis of *H. pylori* (**Fig. 2B**).
169 From these results, we conclude that the AapA1 toxin is specifically targeted to the inner
170 membrane of *H. pylori*.
171
172 **AapA1 toxin has a minor impact on *H. pylori* membrane potential and intracellular ATP**
173 **content**
174 Considering the membrane localization of the toxin, we hypothesized that AapA1
175 expression could affect the membrane potential and by consequence the ATP content of the
176 cells. To explore this possibility, *H. pylori* cells harboring pA1-IsoA1, pA1* or pA1 plasmids
177 were taken at different culture time points, stained with a membrane potential sensitive dye
178 (MitoRed CMXROS) and analyzed by microscopy (**Fig. 2C**). Bacteria harboring either an
179 empty plasmid (B128), pA1-IsoA1 or pA1* exhibit a uniform MitoRed CMXROS
180 fluorescence pattern indicative of membrane integrity. For *H. pylori* cells overexpressing
181 AapA1 and converting to coccoids, the fluorescence pattern progressively evolves from
182 uniform to that of discrete foci, suggesting local changes in membrane permeability. No such
183 foci were observed with coccoids from aging WT strain cultures (72h) or with cells treated
184 with 3,5,3',4'-tetrachlorosalicylanilide (TCS), an effective *H. pylori* protonophore (22) that
185 causes an overall MitoRed CMXROS fluorescence loss due to massive dissipation of
186 membrane potential (**Fig. 2C**). Similar results were obtained with the membrane potential
187 sensitive dye DIOC-5, confirming the local effect of AapA1 on *H. pylori* inner membrane
188 (**Fig. S3**). These data indicate that when the AapA1 toxin is expressed in *H. pylori*, the
189 membrane permeability is not globally compromised but probably locally perturbed.

Next, the ATP content of *H. pylori* strains carrying either pA1-IsoA1 or pA1 was measured from total metabolites extracted at different culture time points and quantification by a luciferase based-assay (**Fig. 2D**). After 6h of culture, IPTG induction had a minor effect on cellular ATP content of both strains as compared to the drastic consequences observed with the TCS control. Note that at 6h of culture with IPTG, most of the pA1-containing cells have already transformed into coccoids. After 16h, the overall ATP content strongly drops in both strains and IPTG induction causes an additional weak decrease that is poorly changed upon toxin expression by pA1 (**Fig. 2D).**

Taken together, these results show that the AapA1 toxin locally perturbs the *H. pylori* membrane potential with no major consequences on the cellular ATP content. We conclude that dissipation of membrane potential is not the major cause of toxin-induced bacterial growth arrest.

Ultrastructural analysis of toxin-induced coccoids

For the first time, cryo-electron microscopy (cryo-EM) was used to visualize *H. pylori* coccoids in near-native states. Using this method, we compared exponentially growing bacteria, toxin-induced coccoids and aging coccoids (70h growth) (**Fig. 3**). In exponential phase, the characteristic helicoidal shape of *H. pylori* (strains B128 WT, 4h and pA1-IsoA1, 4-8h) was perfectly visible with a uniformly contrasted cytoplasm surrounded by two dense layers of membranes and multiple flagella. The periplasm of variable thickness surrounding the cell is distinguishable as the low-density space between the inner and outer membrane. Strains expressing the toxin (pA1 at 4-8h) have intact flagella and are visible in two major morphotypes. In the first “U” shaped morphology, a round intact outer membrane surrounds a bent intact inner membrane. The second morphotype corresponds to round coccoids of a diameter of approximately 1µm, with visible integrity of both membranes and a central

uniformly stained dense cytoplasm. This second morphotype is similar to that of aging coccoids from the WT strain (70h).

In conclusion, CryoEM images revealed that the toxin-induced *H. pylori* coccoids have no visible defect in membrane integrity and are ultrastructurally similar to aging coccoid forms.

Modification of peptidoglycan composition upon transformation of *H. pylori* into coccoids

Our data showed that the AapA1 toxin targets *H. pylori* inner membrane without causing significant membrane potential collapse and without visible loss of integrity. Therefore, we tested whether the toxin-induced cell shape transformation could be associated with modifications in the cell wall and thus in peptidoglycan (PG) composition. PG extracted from B128 WT strain in exponential phase or after 72h growth (aging coccoids) was compared to PG from the pA1 strain induced during 6 and 16h (toxin-induced coccoids). Samples were digested with mutanolysin and subjected to HPLC/MS analyses. The relative abundance of muropeptides in each sample was calculated according to Glauner *et al.* (23) (**Table S1**). When compared to PG of helicoidal *H. pylori*, both "aging" and "toxin-induced" coccoids present similar changes in dipeptide and tripeptide monomers with a stronger effect of toxin-induction at 16h. Coccoids after 16h induction present a 3-fold increase in dipeptide monomers concomitant with tri- and pentapeptide monomers reduction. These data indicate that toxin-induced and aging coccoids undergo similar PG modifications, compatible with a looser PG macromolecule, and suggest that they might be generated by similar mechanisms.

Kinetics of the toxin-induced *H. pylori* morphological transformation assessed by live cell imaging

To progress in our understanding of the morphological conversion of *H. pylori*, we monitored the entire process of *H. pylori* toxin-induced conversion by live cell time-lapse

241 microscopy under physiological microaerobic conditions in a temperature-controlled chamber.
242 The *H. pylori* B128 strain tested constitutively expressed cytoplasmic GFP, was impaired in
243 motility (by deletion of *flaA* encoding the major flagellar protein) and carried the inducible
244 toxin-expressing plasmid pA1. Individual live *H. pylori* bacteria were monitored in agarose
245 pad by both phase contrast and fluorescence microscopy.

246 First, the general growth features of the strain were established in the absence of the IPTG
247 inducer. Under these conditions, statistics of the data collected showed that the strain has a
248 mean doubling time of 165 min (indicative of optimal growth conditions) with an initial
249 bacterial length of 2.1µm after division and a maximum length prior to division of 3.7µm (**Fig.**
250 **S4**). In a second round of experiments, the inducer was added to the pad and snapshots of the
251 cells were taken at intervals of 10 or 15min during 10h (**Fig. 4**). A total number of 63 cells
252 were analyzed from 4 independent experiments, the data are statistically significant. Two
253 representative movies can also be viewed in **Fig. S5**. Only 14 cells did not show visible cell
254 shape modification while the majority (49 bacteria) went through sequential morphological
255 transformations. We classified the transformation steps into 3 categories: "bending" (U-
256 shaped), "pseudo-coccoid" (quasi-round bacteria) and "donut" (fully developed coccoids) and
257 quantified them (**Fig. 4)**. At 185±8.0 min post-induction, 77% of the cells analyzed had
258 undergone bending. One hundred minutes later, only 12 cells were still at this stage while the
259 others had turned into pseudo-coccoids. Finally, one third of the analyzed cells (21 cells)
260 ended up in the round "donut" shape at 420±25.2 min after toxin-induction.

261 Most interestingly, the length of bacteria just before they entered the first morphological
262 transformation (bending) was 3.48±0.08µm, which precisely corresponds to the maximum
263 length we measured before *H. pylori* division. In addition, we observed many examples of
264 two bacteria that were dividing but not yet separated and from which one out of the two
265 underwent morphological transformation (see movie in **Fig. S5**). This analysis gave us a
266 dynamic picture of the morphological transformation of *H. pylori.* Importantly, this analysis

strongly suggests that the morphological transformation is consecutive to a toxin-induced perturbation of cell division, through a mechanism that is still to be defined.

Toxin-antitoxin imbalanced expression upon oxidative stress

We then searched what physiological signal could trigger the induction of the AapA1 toxin expression in *H. pylori*. First, the respective activities of individual *aapA1* and *IsoA1* promoters were measured with chromosomally expressed transcriptional *lacZ* fusions (**Fig. S1**). Under normal growth conditions, ß-galactosidase activities indicated that the antitoxin promoter has a 10-fold stronger activity than the toxin promoter (**Fig. 5A**). This result is consistent with type I TA features where the antitoxin RNA is strongly expressed (but highly labile) compared to the more stable toxin transcript that is expressed at a lower level (7, 8, 18). The *lacZ* fusions were then used to follow the activity of the two promoters during *H. pylori* growth and to search for conditions relevant to *H. pylori* life-style that could lead to imbalanced expression of the two promoters. Only a slight increase in activity of both promoters was observed over time of growth (**Fig. 5A**). No significant differential expression of the promoters was observed upon acid, antibiotic stress or during exposure to high nickel concentrations (**Fig. S6**). In contrast, oxidative stress induced by hydrogen peroxide (H_2O_2) resulted in a strong specific decrease in the *IsoA1* promoter activity while, at the same concentration, the toxin promoter activity was marginally reduced (**Fig. 5B**). Exposure to paraquat, another oxidative stress agent, resulted in a comparable strong decrease of both promoters. The expression patterns and stability of the *aapA1* and *IsoA1* transcripts were then analyzed by Northern Blot with total RNA extracted at different time points after rifampicin addition. As shown in **Fig. 5C** and **Fig. S7**, the *aapA1* transcript was detected as a 175 nucleotide-long band with an estimated half-life of approx. 120min. In contrast, the 75 nt *IsoA1* full length transcript declines much faster, with an estimated 25min half-life, and the production of an approx. 50 nt short processed form. Upon hydrogen peroxide exposure, the

293 half-life of the AapA1 transcript was not significantly modified while we observed a more
294 rapid depletion of the full-length *IsoA1* transcript with an almost immediate accumulation of
295 the processed form (**Fig. 5C**). From three independent experiments, we quantified the relative
296 amounts of the transcripts under normal growth conditions versus H_2O_2 exposure during 120
297 min after rifampicin addition (**Fig. 5D**). No significant change was observed for the *aapA1*
298 transcript while H_2O_2 exposure resulted in a diminished half life of the *IsoA1* full length
299 transcript and in an imbalanced ratio of *IsoA1* in favor of its processed form (**Fig. 5D**). Taken
300 together, these results show that H_2O_2 causes both diminished *IsoA1* transcription and
301 increased degradation of *IsoA1* full-length transcript. These observations suggest that, by
302 decreasing the amounts of antitoxin transcript, exposure to oxidative stress favors translation
303 of the AapA1 mRNA and thus toxin production.
304
305 **Oxidative stress induction of coccoids: are class A Type I TA the only effectors ?**
306 Since we established that oxidative stress results in imbalanced expression in favor of the
307 expression AapA1 toxin, we examined the consequences of exposure to this condition on *H.*
308 *pylori* morphology and viability. Upon H_2O_2 oxidative stress, we observed a rapid
309 transformation into coccoids (approx. 6h) in strain B128. This strain contains six class A type
310 I TA systems, the A2 locus being inactive (**Fig. S8**). To assess their role, we constructed
311 mutants carrying deletions of each of its active AapA/IsoA TA loci, Δ*A1*, Δ*A3*, Δ*A4*
312 (including deletion of both *A4-1* and *A4-2* tandem systems), Δ*A5*, Δ*A6* or of the five loci
313 collectively (Δ*5*) using a non-marked deletion strategy (24). Under normal conditions, the
314 growth rate, culturability and kinetics of occurrence of coccoids of the different mutants was
315 similar to that of the parental strain (**Fig. S9**). Upon H_2O_2 oxidative stress, the Δ5 mutant
316 strain displayed similar kinetics of conversion to coccoids when compared to the parental
317 strain.

318 This shows that oxidative stress is triggering transformation into coccoid but that the type I
319 toxins are not the only effectors. TA systems have been shown to play a role in persister cell
320 formation under stress conditions (7, 8). Therefore, the number of persisters after exposure to
321 hydrogen peroxide was measured for the ΔA1 and Δ5 mutants and compared to the parental
322 strain (**Fig. S9**). No significant difference was observed, suggesting that, upon hydrogen
323 peroxide stress, the class A TA systems are not promoting viable persisters in *H. pylori*.
324

Discussion

Here we established that the expression of a small toxin from a toxin-antitoxin system triggers a massive and rapid morphological transformation of the spiral-shaped *H. pylori* bacterium into round coccoid cells. Transformation of spirals into coccoids has been observed after extended *H. pylori* growth (>70h, aging coccoids) or upon stress conditions (14) but the process itself was poorly characterized. The toxin (AapA1) is a small hydrophobic peptide of a type I TA system that we showed here to target *H. pylori* inner membrane without being secreted. Toxins of type I TA system from other organisms such as *Escherichia coli*, *Bacillus subtilis* or *Staphylococcus aureus* have been shown to localize to the inner membrane but there are no reports on induction of major cell shape modifications (8, 25-27). The *E. coli* TisB (28) and the *S. aureus* PepA1 (29) toxins act by creating membrane pores (similar to phage holins) thereby disrupting the membrane potential, drastically impairing ATP synthesis and depending on the toxin concentration, either leading to the formation of persisters or to cell death (8, 27). One notable exception is the BsrG/SR4 Type I TA system of *B. subtilis* (26). The BsrG toxin was found to target the membrane without causing destruction or affecting the Proton Motive Force but it rather directly interferes with the cell envelope biosynthesis, indirectly delocalizes the cell-wall synthesis machinery and ultimately triggers bacterial autolysis (26). There are now two examples of type I TA hydrophobic toxins (BsrG and AapA1 reported here) that do not act by permeabilizing the membrane and probably reflect a novel mode of action for small peptidic toxins.

Using for the first time cryo-EM, we observed that toxin-induced *H. pylori* coccoids present neither visible membrane disruption nor pores even 8h post toxin induction and are ultrastructurally comparable to 70h-old aging coccoids. The membrane potential of coccoids was not dissipated despite the fact that the toxin induces local perturbation of the membrane. This is in contrast with a previous study that reported a total loss of membrane potential in *H. pylori* aging coccoids, associated with a complete loss of membrane integrity (30). Unlike the

effects of the TisB toxin in *E. coli* (28), we found that the ATP content in our *H. pylori* toxin-induced coccoids is marginally affected and drops only after prolonged culture, as it is the case for spiral-shaped cells (31).

Toxins expressed by TA systems cause growth arrest by interfering with conserved vital cellular processes such as translation, division or peptidoglycan (PG) synthesis (8, 27). In bacteria, PG cell-wall dictates cell shape. We found that coccoid transformation was accompanied by changes in PG composition. Indeed, when compared to spirals, coccoids have a three-fold increase in dipeptide monomers concomitant with a tri- and pentapeptide monomers reduction. These changes are comparable to those previously reported for "aging" *H. pylori* coccoids (32) and were confirmed here. Our results point to a reduction in the potential for generating new cross-bridges in the PG; this is compatible with a looser PG macromolecule and could explain the morphological transition to coccoids. The PG metabolism has been extensively studied in *H. pylori* (33). The modifications we observed in coccoids suggest activation of at least three sequential *H. pylori* PG hydrolase activities. A D,D-carboxypeptidase that transforms pentapeptides into tetrapeptides; HdpA/Csd3 is the only reported such enzyme (34). A L,D-carboxypeptidase that transforms tretapeptides into tripeptides carried out by Csd6, a member of the L,D-transpeptidases (33). Finally, a (g)-glutamyl-diaminopimelate carboxypeptidase generating dipeptides from tripeptides carried out by Cds4, a member of the M14-zinc metallopeptidases (33). We previously showed that these three PG modifications are blocked in a mutant deficient in AmiA, a putative *H. pylori* amidase and that an *amiA* mutant fails to transform into coccoids (35). Therefore, we propose that AmiA could be a central hub for the functionality of a PG hydrolase complex including AmiA, HdpA, Csd4 and Csd6. In this case, the AapA1 toxin would interfere with the function of this complex by causing abnormal activation of their enzymatic activities.

Life imaging analysis of the toxin-induced conversion of *H. pylori* spirals into coccoids suggested that the AapA1 toxin interferes with cell division. This is also consistent with a

central role of AmiA in the conversion, indeed this enzyme was shown to be essential for the separation of daughter cells (35). In *E. coli*, the CbtA toxin of a type IV TA system was found to inhibit cell division and cell elongation via direct and independent interactions with FtsZ and MreB (36). More work is needed to identify the molecular target(s) of the AapA1 toxin.

Under normal conditions, as for all TA systems, the *IsoA1* antitoxin potently inhibits the AapA1 toxin, by preventing its expression through a multilayered mechanism (20). We searched for physiological conditions that could result in toxin expression. We found that oxidative stress, generated by H_2O_2, causes a rapid and specific decline in the levels of IsoA1 antitoxin full-length transcript by reducing both its promoter activity and enhancing its degradation through a mechanism that remains to be precisely defined. Imbalanced expression of the AapA1/IsoA1 system in favor of the toxin mRNA should lead to toxin expression. Accordingly, we observed that H_2O_2 causes a rapid conversion of *H. pylori* into coccoids resembling those induced by the AapA1 toxin. Prolonged exposure to aerobic conditions was previously reported to lead to the coccoid formation, however, in that case these cells lost their membrane integrity (37). Regulation of type I TA systems in response to stress had been observed in other species. For the *bsrE*/SR5 type I system of *B. subtilis*, the SR5 antitoxin is affected by pH, anoxia and iron limitation while the BsrE toxin is sensitive to temperature shock and alkaline stress (38). In *S. aureus*, the SprA1/SprA1$_{AS}$ system is induced in response to acidic or oxidative stresses (29). In *E. coli*, several type I toxins are induced by the SOS response (7), a system that does not exist in *H. pylori*.

The biological function of *H. pylori* coccoids is still a matter of debate. Coccoids are observed in prolonged *in vitro* cultures and induced by stress conditions, mostly aerobic, anaerobic culture or exposure to antibiotic or oxidative stress. However, these reports are difficult to compare since no standard procedure was used and analysis was most of the time performed after more than a week stress exposure (14, 30, 39). *H. pylori* coccoids are non-culturable cells under standard laboratory growth conditions. Our analysis of both toxin-

403 induced and 70h aging coccoids are in favor of their viability despite their "unculturability".
404 We argue that contradictory conclusions on viability refer to "damaged" or so-called
405 "fragmented" coccoid forms corresponding to membrane-less bacteria in prolonged *H. pylori*
406 cultures (30). In favor of coccoid viability are previous reports showing that coccoids express
407 virulence factors (14) and are capable, like spirals, of binding to host cells and inducing
408 cellular changes (40). *H. pylori* coccoids were also visualized in human gastric biopsies (41),
409 probably as part of biofilms (39). In mice, coccoids induce gastritis (42) and can revert to
410 colonizing spiral bacteria (43). Taken together, these observations suggest that coccoids are
411 "dormant" viable forms of *H. pylori* that recover during host infection and might play a role
412 in transmission or in treatment failure. In agreement with this view, Chaput *et al.* (35) showed
413 that coccoids present decreased activation of NF-kB and might allow the bacterium to escape
414 the host immune response.

415 We showed that *H. pylori* coccoids are induced by a class A type I TA toxin and by
416 oxidative stress probably through the imbalanced expression of TA systems. During infection,
417 *H. pylori* is indeed exposed to harsh oxidative stress as a consequence of the chronic
418 inflammation it generates (44). Deletion of the five "class A" Type I TA clusters of *H. pylori*
419 did not preclude the oxidative stress induction of coccoids nor did it change the number of
420 persister cells. We concluded that these toxins are probably not the only triggers of coccoid
421 transformation and suggest that the two other classes of chromosomally-encoded type I TA
422 systems (B and C representing 9 systems) might also be important.

423 Dormant/persister bacteria present enhanced tolerance to antibiotics and it has been shown
424 that they can be induced by TA systems (7, 8), although other mechanisms resulting in
425 lowered ATP content are also associated with their occurrence (11). We hypothesize that TA-
426 induced *H. pylori* coccoids are dormant bacteria and, as previously proposed, that non-
427 culturable cells and "classical" dormant bacteria/persisters are part of a shared "dormancy

continuum" (45). In our model, this continuum would depend on the intracellular toxin concentration as already suggested (46).

Stress-induced morphological transformation of bacteria into non-culturable coccoid-like cells has been reported in at least 85 bacterial species among which important bacterial pathogens such as *Campylobacter jejuni, Vibrio cholerae* or *Salmonella typhimurium* (16). For these organisms, the inducing trigger and function remains to be characterized. We postulate that these forms are dormant bacteria and that our findings on *H. pylori* might be more generally relevant and play important roles in recurrent and persistent bacterial infections.

438

439 **Figure legends**

440 **Figure 1: Expression of the AapA1 toxin from the AapA1/IsoA1 TA system induces**
441 **growth arrest and transformation of *H. pylori* strain B128 into coccoids.**

442 **A)** Genetic organization of AapA1/IsoA1 locus in *H. pylori* B128 strain with the AapA1
443 transcript encoding the toxin and the *IsoA1* antitoxin RNA. Below is the representation of the
444 inserts of the three plasmids constructed by Arnion *et al* (20) and used in this study, each
445 derived from the pILL2157 *E. coli/H. pylori* vector (21). These inserts are expressed under
446 the control of an IPTG inducible promoter. Plasmid pA1-IsoA1 expresses both the toxin and
447 the first 30 nucleotides of the *IsoA1* RNA antitoxin. In pA1, the promoter region of IsoA1
448 was mutated without affecting the amino acid sequence of AapA1. Plasmid pA1* was derived
449 from pA1 and contained an additional mutation inactivating the start codon of AapA1.

450 **B) Expression of the AapA1 toxin causes rapid growth arrest of *H. pylori* strain B128.**
451 Growth kinetics of *H. pylori* B128 strains carrying each of the three plasmids illustrated in
452 panel A, grown in the absence (black symbols) or in the presence of 1mM IPTG (empty
453 symbols) that was added at the time indicated by an arrow (16h).

454 **C) Expression of the AapA1 toxin induces transformation of *H. pylori* into coccoids.**
455 Microscopy analysis of the *H. pylori* B128 strains carrying each of the three plasmids after
456 growth in the absence of IPTG or at 4 and 8h following IPTG addition. *H. pylori* membranes
457 were stained with the lipophilic dye TMA-DPH. Phase-contrast and fluorescence images are
458 respectively represented on the upper and bottom panel. The scale bar corresponds to 1μm.

459

460 **Figure 2: AapA1 toxin targets *H. pylori* inner membrane, weakly disturbs the bacterial**
461 **membrane potential and poorly affects intracellular ATP content.**

462 **A) AapA1 toxin localizes to the *H. pylori* inner membrane.** Western blot analysis of total
463 extracts (T), soluble extracts (SE), inner membrane (IM) and outer membrane (OM) fractions

prepared from *H. pylori* B128 strain expressing either a SPA tagged-AapA1 toxin (pA1-SPA) under control of an IPTG-inducible promoter or carrying plasmid pA1* as a negative control. The fractionation procedure was validated with antibodies against the following control proteins, PBP2 for the inner membrane, AlpA for the outer membrane and NikR for the cytoplasm. In **Fig. S2**, we show that a A1-GFP fusion expressed either from the chromosome of B128 or from a plasmid also localizes at the inner membrane.

B) In live cells, AapA1-GFP localizes as discrete foci around the *H. pylori* membrane. Strain B128 expressing the AapA1-GPF fusion protein was analyzed on agarose pads by fluorescence microscopy 6h after IPTG-induction. Membranes were stained with TMA-DPH lipophilic dye. The membrane association of AapA1-GPF was quantified by measuring the fluorescence intensity profile perpendicular to the length axis of *H. pylori*. The graph shows the average fluorescence intensity profiles with standard deviation (n=25). The fluorescence maxima separated by 0.5 μm, correlate with the *H. pylori* cell width.

C) Analysis of the effect of the AapA1 toxin on *H. pylori* membrane potential. MitoRed CMXROS, a membrane potential reactive dye was used to analyze live *H. pylori* B128 strains expressing each of the three plasmids illustrated in **Fig. 1**. Cells were grown in presence or absence of 1mM IPTG and analyzed on agarose pads at 0, 4, 8 and 24 h after IPTG addition. While uniformly stained by the MitoRed CMXROS in the absence of IPTG, cells expressing the toxin (pA1) present discrete foci of stronger fluorescence suggesting a local disturbance of the membrane potential. For comparison, a 72h-old culture of B128 WT strain forming "aging" coccoids was also analyzed. As a positive control of membrane potential loss, 4h-old B128 WT cells were analyzed after treatment or not with TCS (3,3',4',5-Tetrachlorosalicylanilide) an *H. pylori* active protonophore. Bar scale represents 1μm.

D) Measurement of intracellular ATP content. Intracellular ATP was extracted from B128 strains harboring pA1-IsoA1 or pA1 after 6 or 16h growth in the presence or absence of IPTG. B128 WT strain treated with 500μM of TCS

490 protonophore was used as a positive control. ATP concentrations were determined using a
491 luciferase-based assay (BacTiter-Glo™, Promega). Results from 3 independent experiments
492 performed in triplicates are shown. Error bars represent the standard deviation, with * and **
493 indicating that the mean value is significantly different, * corresponds to $P < 0.05$, ** to $P <$
494 0.01, *** to $P < 0.001$ and NS corresponds to non-significant, ($P > 0.05$).
495
496 **Figure 3: Ultrastructural analysis of toxin-induced coccoids and "aging" coccoids by**
497 **cryo-electron microscopy.**
498 Cryo-electron microscopy was used to compare "aging" coccoids (70 h-old cultures) and
499 exponentially growing B128 strains carrying plasmid pA1-IsoA1 or pA1 grown for 4 or 8h in
500 the presence of IPTG. Expression of the toxin results in the formation of U-shaped bacteria at
501 4h and round coccoids cells at 8h with visible intact bacterial cell envelop similar to the aging
502 coccoids. Scale bar represents 1μm.
503
504 **Figure 4: Time-lapse microscopy of *H. pylori* conversion to coccoid upon toxin**
505 **expression.**
506 Live cell time lapse microscopy was used to record, during 10 hours, the morphological
507 modifications of individual *H. pylori* B128 strain cells after IPTG-induction of the AapA1
508 toxin. Phase-contrast and fluorescence images of one example of these kinetics are presented.
509 Scale bar represents 2μm. Three major phenotypes were observed; "bending", "pseudo-
510 coccoids" and "donut". Statistics (median and mean ± SEM) on the total number of analyzed
511 cells and the precise timing to reach the phenotypes are presented. SEM corresponds to
512 standard error of the mean. Representative movies of the transformation can be seen in **Fig.**
513 **S5**.
514

Figure 5: Oxidative stress generated by hydrogen peroxide results in decreased antitoxin promoter activity and promotes *IsoA1* transcript processing.

A) Activity of the AapA1 and IsoA1 promoters as a function of growth.

β-galactosidase activities (expressed in Miller units) measured with *H. pylori* B128 strain carrying chromosomal P*aapA1-lacZ* and P*IsoA1-lacZ* fusions after 6, 24 and 48h growth. Results from 3 independent experiments performed in duplicates are shown. Error bars represent the standard deviation, with * ($P < 0.05$) and ** ($P < 0.01$) indicating that the mean values are significantly different and NS indicating that they are not significantly different ($P >0.05$). The activity of the toxin fusion (*aapA1-lacZ*) is about ten times that of the antitoxin fusion (*IsoA1-lacZ*) and the activity of both promoters slightly increases as a function of growth.

B) Oxidative stress generated by H_2O_2 decreases antitoxin promoter activity.

β-galactosidase activities expressed by P*aapA1-lacZ* and P*IsoA1-lacZ* fusions were measured after 6h treatment with oxidative stress generators, paraquat (5, 50 and 500 µM) and H_2O_2 (0.03 and 0.3%). β-galactosidase activities are presented as ratio (expressed in %) of activities measured with stress versus activities of untreated samples. Hydrogen peroxide strongly decreases the expression of the P*IsoA1-lacZ* fusion. Results from 3 independent experiments performed in duplicates are shown. Error bars represent the standard deviation, with * ($P < 0.05$), ** ($P < 0.01$), *** ($P <0.001$) indicating that the mean values are significantly different and NS that they are not significantly different ($P >0.05$).

C) Determination of AapA1 mRNA and IsoA1 RNA half-lives in *H. pylori* strain B128 under normal conditions and upon hydrogen peroxide exposure.

Northern blots of total RNA from B128 WT strain grown under normal conditions or exposed to 1% hydrogen peroxide, extracted at the indicated times after addition of 80 µg/ml rifampicin. Five µg of RNA were loaded in each lane and the membranes were probed with

[γ-^{32}P] ATP-labeled oligonucleotides specific to the following RNAs, *aapA1*, *IsoA1* and 5S rRNA as a loading control. In the presence of H_2O_2, the half-live of *IsoA1* transcript is diminished in favor of the processed *IsoA1* form.

D) Hydrogen peroxide promotes *IsoA1* transcript processing.

Graphic representation of the effects of hydrogen peroxide exposure on the amounts of *aapA* and *IsoA1* transcripts as well as on *IsoA1* processing during 120 min after rifampicin addition. The relative amounts of *aapA1* (upper graph) and full length (FL) *IsoA1* (middle graph) RNAs versus 5S rRNA are shown. The lower graph presents the relative amounts of the two forms of *IsoA1*, full length (FL) versus the processed form. The results of 3 independent experiments are shown, error bars represent the standard deviation analyzed by two-way ANOVA multiple comparisons.

552

553 **Acknowledgments**

554 This work was funded by the Agence National de la Recherche (ANR 09 BLAN 0287 01 and
555 ANR 12 BSV5-0025-02), the Laboratoire d'Excellence IBEID (Integrative Biology of
556 Emerging Infectious Diseases) Grant ANR-10-LABX-62-IBEID from the French
557 government's Investissement d'Avenir program and the Pasteur-Weizmann Consortium of
558 "The Roles of Noncoding RNAs in Regulation of Microbial Life Styles and Virulence". LEM
559 was funded by a Roux fellowship of the Institut Pasteur and by a Carnot MI fellowship. AR
560 was supported by post-doctoral fellowship from the Labex IBEID (10-LABX-62-IBEID). We
561 also thank Janssen for financial support. We are grateful to F. Darfeuille and H. Arnion for
562 the gift of plasmids and to W. Fischer for the gift of anti-AlpA antibodies. We also appreciate
563 the expertise and help of A. Chery-Faleme, M. Fromont-Racine and A. Jacquier with
564 Northern blotting and of R. Wheeler for peptidoglycan extraction. We thank M. Denic, S.
565 Kumar and A. Tejada-Arranz for comments on the manuscript and J. Berry for discussions.
566 Finally, we thank M. Nilges and the Equipex CACSICE for providing the Falcon II direct
567 detector.

568

Material and Methods

Bacterial strains and growth conditions

The *H. pylori* strains used in this study (Suppl **Table S2**) were all derived of strain B128 (47) (48). Plasmids (suppl **Table S3**) used to create or complement *H. pylori* mutants were constructed and amplified using *E. coli* One-Shot TOP10 or DH5α strains (Thermofisher). *H. pylori* strains were grown on Blood Agar Base 2 (Oxoid) plates supplemented with 10% defibrinated horse blood and with the following antibiotics-antifungal cocktail: amphotericin B 2.5 $\mu g.ml^{-1}$, polymyxin B 0.31 $\mu g.ml^{-1}$, trimethoprim 6.25 $\mu g.ml^{-1}$ and vancomycin 12.5 $\mu g.ml^{-1}$. Selection of *H. pylori* mutants was performed using kanamycin 20 $\mu g.ml^{-1}$, Streptomycin 10$\mu g.ml^{-1}$, Apramycin 10$\mu g.ml^{-1}$ or chloramphenicol 8 $\mu g.ml^{-1}$. For liquid cultures, we used Brain Heart Infusion (BHI) broth (Oxoïd) supplemented with 10% Fetal Calf Serum (FCS) (Eurobio), the antibiotics-antifungal cocktail and the selective antibiotic when necessary. *H. pylori* cells were grown at 37°C under microaerophilic atmosphere conditions (6% O_2, 10% CO_2, 84% N_2) using an Anoxomat (MART Microbiology) atmosphere generator. When indicated, 1mM of isopropyl ß-D-1-thiogalactopyranoside (IPTG, EuroMedex) was added to agarose pads or culture media.

Molecular techniques

Molecular biology experiments were performed according to standard procedures and the supplier (Fermentas) recommendations. NucleoBond Xtra Midi Kit (Macherey-Nagel) and QIAamp DNA Mini Kit (Qiagen) were used for plasmid preparations and *H. pylori* genomic DNA extractions, respectively. PCR were performed either with Taq Core DNA polymerase (MP Biomedicals), or with Phusion Hot Start DNA polymerase (Finnzymes) when the product required high fidelity polymerase. The pGEM-T easy vector systems (Promega) was

used to construct in *E. coli*, the suicide plasmids that served for markerless deletions of TA systems in *H. pylori*.

Construction of H. pylori strains carrying mutation or plasmids

Mutations of *H. pylori* were introduced into strain B128 either WT or a streptomycin resistant variant B128 *rpsL1* for markerless mutagenesis (24, 49). Chromosomal deletions of the *AapA1*/IsoA1 locus, of the *flaA* gene, or of the different class A TA loci were performed either by insertion of a selectable antibiotic resistance marker to disrupt or replace the gene of interest or when necessary, by the markerless counter-selected mutagenesis strategy (24, 49). Plasmids were derived from the pILL2157 *E. coli/H. pylori* shuttle vector that contains an IPTG-inducible promoter (21). Deletions were introduced by allelic exchange using suicide plasmids (see suppl **Table S3**) or PCR fragments. Introduction of plasmids and construction of *H. pylori* mutants were obtained by natural transformation and selection with the corresponding antibiotic as described previously (24). PCR and sequencing of the regions of interest were used to validate the introduction of plasmids, deletion of genes of interest and correct insertion of fusions. Primers used for these constructs or their validation are listed in Suppl **Table S4.**

Confocal Fluorescence Microscopy

Fluorescence microscopy was performed with an Axio Observer microscope (Zeiss) equipped with an Axiocam camera under an X100 magnification. Acquisition images was performed using the axiovision software. Images were cropped and adjusted using ImageJ 1.47v software. *H. pylori* B128 strains were grown in BHI medium with chloramphenicol (8 µg/ml) to maintain the plasmids. IPTG was added to the culture and samples were taken at different time-points, concentrated by 2 min centrifugation at 3000 x g and washed twice with PBS buffer. Cells were immobilized using 2% (wt/vol) agarose pads containing PBS before

being imaged. In **Fig. 1C**, cell membranes were stained with 0.01 mM TMA-DPH (1-(4-trimethylammoniumphenyl)-6-phenyl-1,3,5-hexatriene p-toluenesulfonate, Euromedex). Membrane potential was revealed with 25nM MitoTracker®Red CMXROS (Invitrogen) in **Fig. 2C** and with 1µM DIOC-5 (3) (3,3-Dipentyloxacarbocyanine iodide, Interchim) in **Fig. S3**. For the membrane potential analysis, the negative control was obtained by treatment with the protonophore 500µM TCS (3,3',4',5-Tetrachlorosalicylanilide; Fisher scientific).

Fractionation and Immunoblotting

The protocol of *H. pylori* fractionation was adapted from (50). *H. pylori* strains were grown in the absence or presence of 1mM IPTG. When cultures reached OD_{600} 0.8, cells were harvested by centrifugation, washed twice in phosphate-buffered saline medium (PBS) prior to their disruption by sonication in Buffer 1, 10mM Tris-HCl, pH7.5 containing 5mM ß-mercaptoethanol and proteases inhibitors (cOmplete™, EDTA-free Protease Inhibitor Cocktail, Roche). Cell debris were removed by centrifugation (10 min, 16,000 x *g*, 4°C) and supernatants containing the soluble extract and membrane fractions were collected as total extracts. Samples of total extracts were frozen and the remaining supernatants were subjected to ultracentrifugation (125,000 x *g*, 45 min, 4°C). Samples from the supernatant containing the cytoplasm and periplasm were collected and frozen while pellets containing total membranes were resuspended in buffer 1 supplemented with 1% N-lauroylsarcosine (Buffer 2) prior to be ultracentrifuged (125,000 x *g*, 45 min, 4°C). Samples of inner membrane fractions from supernatants were frozen. Outer membrane pellets were washed twice in buffer 2 to avoid inner membrane fractions contamination prior to freezing. In each fraction, protein amounts were calibrated using the Bradford DC Protein Assay (Biorad) with bovine serum albumin (BSA) as a standard. For each cellular compartment, equal protein amounts were loaded and separated on a 4-20% Mini-Protean TGX precast protein gel (BioRad) and subsequently electrotransferred on a polyvinylidene difluoride (PVDF) membrane (Biorad).

The *H. pylori* proteins PPB2, AlpA and NikR as well as the fusion protein A1-SPA or A1-GFP were detected with rabbit polyclonal antibodies α-PBP2 (51), α-AlpA (50), α-NikR (52); with mouse monoclonal anti-FLAG M2 antibody (Sigma-Aldrich) or with goat anti-GFP-HRP antibody (Abcam) at the respective dilutions of 1:2,000, 1:1,000, 1:100 and 1:1,000 or 1:5,000. Goat anti-rabbit IgG-HRP (Santa Cruz) and ECL anti-mouse IgG Horseradish Peroxydase (Amersham) were used as secondary antibodies and the detection was achieved with the ECL reagent (Pierce).

ATP extraction and assay

Exponentially growing *H. pylori* cells (6h of culture OD_{600nm} 0.35) and stationary growing cells (16h, OD_{600nm} 3) were harvested by centrifugation at room temperature for 4 min at 5000*g*. Metabolites from the resulting cell pellets were extracted immediately using 300µL of a solvent mixture of Acetonitrile/Methanol/H_2O (40/40/20) for 15min at 4°C and 10min at 95°C. Mixtures were subsequently spun in a microfuge for 5 min at maximum speed and 4°C to separate insoluble materials from the extracted metabolites. The resulting pellets were then re-extracted twice with 200 µL of solvent at 4°C. The supernatants were pooled to yield 700 µL of final extract. Metabolites were lyophilized and subsequently diluted in water for ATP assays. ATP content was determined by a luciferase based ATP bioluminescence assay kit (BacTiter-Glo™ Microbial cell viability assay, Promega). Luminescence values were determined using a 10 sec RLU signal integration time and measured using a Centro XS^3 LB960 Luminometer (Berthold Technologies). ATP concentrations were calculated based on values determined using serial dilutions of known amounts of ATP and expressed as a function of the OD_{600nm} of the corresponding culture.

Cryo-electron microscopy

Four µL of *H. pylori* bacteria were spotted on glow-discharged lacey grids (S166-3, EMS) or Quantifoil R2/2 (Quantifoil, Germany). The samples were cryo-fixed by plunge freezing at -180°C in liquid ethane using a Leica EMGP (Leica, Austria). Grids were observed at 200kV with a Tecnai F20 (Thermo Fisher Scientific). Images were acquired under low-dose conditions using the software EPU (Thermo Fisher Scientific) and a direct detector Falcon II (Thermo Fisher Scientific).

Time-lapse microscopy

Confocal analysis of live cells was performed as previously described (53). Twenty µL of exponentially grown bacteria (10^5 cells) suspended in BHI with or without 1mM IPTG were deposited on 35mm glass bottom Petri dishes. The suspension was covered with BHI medium in 1.5% low melting agarose supplemented with Chloramphenicol (8µg/µl) with or without IPTG (1mM). Live-cell imaging was performed with a Nikon A1R confocal laser scanning microscope system attached to an inverted ECLIPSE Ti (Nikon Corp., Tokyo, Japan) and equipped with an environmental chamber allowing the control of temperature (37°C), humidity (90%) and gas mixture (10% CO_2, 3% O_2). GFP fluorescence images were captured through a Plan APO 60X objective (NA: 1.40) by using optimal spatial resolution settings. The cytoplasm compartment volume was defined by using GFP staining (excitation with 488 nm laser, emission collected with an 500/50 nm filter set). Image captions were performed every 10min during 10h. Statistics were performed on a total of 63 cells from 4 independent experiments. Image treatment and analysis were performed using NIS elements (Nikon Corp., Tokyo, Japan) and ImageJ software.

ß-galactosidase activity assays

B128Δ*AapA1-IsoA1::PaapA1-lacZ-Kan* and B128Δ*AapA1-IsoA1::PIsoA1-lacZ-Kan* strains were grown to OD_{600nm} 0.3 in BHI liquid medium, then divided into two samples, one

of them being submitted to stress conditions during 6h with 5, 50 and 500 µM paraquat (Sigma), 0.03 and 0.3% hydrogen peroxide (Sigma), 20 and 200 mM $NiCl_2$ (Sigma), 0.1 and 1 mg/mL tetracycline, or 0.05 and 0.5 mg/ml rifampicin. Then 0.5ml samples were taken, washed twice with 1X PBS (Phosphate Buffered Saline) and further permeabilized with 100µL Chloroform and 50µl SDS 0.1% in Z buffer containing 70mM $Na_2HPO_4.12H_2O$, 30mM NaH_2PO_4. H_2O, 1mM $MgSO_4$ and 0.2mM $MnSO_4$ (54). Samples were briefly vortexed and incubated at 28°C for 2 min. The ß-galactosidase assay was started by adding 0.5mL ONPG (ThermoFischer) at 4mg/ml and stopped by the addition of 0.5mL 1M Na_2CO_3 when sufficient yellow color was reached. The ß-galactosidase activity is expressed in Miller units (54) and represented in **Fig. 5** and **S6** as percentage of activities relative to the control activity with the corresponding strains not exposed to stress and was calculated from 3 independent experiments performed in duplicates.

Total RNA extraction and Northern blotting

Total RNAs were extracted from 10 mL *H. pylori* cultures (OD_{600} 0.5 -0.9) exposed or not to 1% H_2O_2 using the NucleoSpin miRNA kit (Macherey Nagel) at different time points after 80 µg/mL rifampicin addition (to stop transcription). For Northern blotting, 5 µg of total RNA were separated on 10% Mini protean TBE Urea gel (Biorad) and transferred to Hybond N+ (Amersham Biosciences) membrane susing a Trans-Blot Turbo system (Biorad). A DNA marker was used for size estimation.

Transferred RNA was fixed to the membrane by UV irradiation for 2 min. The membrane was blocked for 45 min at 42°C with ULTRAhyb Hybridization Buffer (Ambion), then 20 µl of 5'-labeled ($\gamma^{32}P$) oligodeoxynucleotides (**Table S4**) were added and the membrane was further incubated overnight at the same temperature. After three washes for 10 min at 65°C with 2x SSC 0.2 % SDS, the membrane was exposed to a phosphorimager screen (KODAK)

and scanned with FLA-9000 Phospho Imager (Fujifilm).

Peptidoglycan extraction and Muropeptides analysis by HPLC/HRMS

Samples (1L) of *H. pylori* B128 WT strain (16h, exponential phase and 72h, "aging" coccoids) and of B128 Δ*aapA1-IsoA1* pA1 strain, induced by IPTG during 6h and 16h, were taken and chilled in an ice-ethanol bath. Crude murein sacculi were immediately extracted in boiling sodium dodecyl sulfate (SDS 4% final). The resulting purified peptidoglycan was digested overnight at 37°C in 12.5 mM sodium phosphate buffer (pH 5.6) supplemented with 100 UI of mutanolysin from *Streptomyces globisporus* ATCC 21553 (Sigma). The reaction was stopped by heat inactivation of the enzyme and insoluble material was removed by centrifugation. Soluble muropeptides were then reduced with sodium borohydride in borate buffer (pH 9). After centrifugation, reduced muropeptides were diluted 20-fold in water-formic acid 0.1% (v/v; solvent A). HPLC/HRMS (High Performance Liquid Chromatography / High Resolution Mass Spectrometry) was performed on an Ultimate 3000 UHPLC (Ultra High Performance Liquid Chromatography) system coupled to a quadrupole-Orbitrap mass spectrometer (Q-Exactive Focus, Thermo Fisher Scientific). Muropeptides were separated on an Hypersil Gold aQ analytical column (1.9 µm, 2.1x150 mm) at 200 µL/min, column temperature at 50°C. Applied linear gradient from 0 to 12.5% acetonitrile + 0,1% (v/v) formic acid (solvent B), followed by increasing to 20% B at 25 min for 5 min, hold 20% B for min and additional 10 min with 100% A for column re-equilibration. Eluted muropeptides were introduced into Q-Exactive instrument, operating in positive ion mode, and then were analyzed in the data-dependent acquisition mode (FullMSddMS2). Data were then processed with the software TraceFinder 3.3 (Thermo Fisher Scientific) for peak areas determination, the relative abundance of muropeptides in each sample was calculated according to Glauner *et al.* (23).

748 **Statistical analysis**

749 The Student's t test was used to determine significance of the means of the data. Error bars
750 represent the standard deviation, with * ($P < 0.05$), ** ($P < 0.01$), *** (P <0.001) indicating
751 that the mean values are significantly different and NS that they are not significantly different
752 ($P >0.05$). SEM corresponds to standard error of the mean. The two-way ANOVA multiple
753 comparisons was used to compare Northern blots bands intensities under different conditions.
754

References

1. Yamaguchi Y, Park J-H, & Inouye M (2011) Toxin-Antitoxin Systems in Bacteria and Archaea. *Annual Review of Genetics* 45(1):61-79.
2. Goeders N & Van Melderen L (2014) Toxin-Antitoxin Systems as Multilevel Interaction Systems. *Toxins* 6(1):304-324.
3. Page R & Peti W (2016) Toxin-antitoxin systems in bacterial growth arrest and persistence. *Nat Chem Biol* 12(4):208-214.
4. Yang QE & Walsh TR (2017) Toxin–antitoxin systems and their role in disseminating and maintaining antimicrobial resistance. *FEMS Microbiology Reviews* 41(3):343-353.
5. Helaine S*, et al.* (2014) Internalization of *Salmonella* by Macrophages Induces Formation of Nonreplicating Persisters. *Science* 343(6167):204-208.
6. Wang X*, et al.* (2011) Antitoxin MqsA helps mediate the bacterial general stress response. *Nat Chem Biol* 7(6):359-366.
7. Berghoff BA & Wagner EGH (2017) RNA-based regulation in type I toxin–antitoxin systems and its implication for bacterial persistence. *Current Genetics*.
8. Harms A, Brodersen DE, Mitarai N, & Gerdes K (2018) Toxins, Targets, and Triggers: An Overview of Toxin-Antitoxin Biology. *Molecular Cell*.
9. Harms A, Maisonneuve E, & Gerdes K (2016) Mechanisms of bacterial persistence during stress and antibiotic exposure. *Science* 354(6318).
10. Goormaghtigh F*, et al.* (2018) Reassessing the Role of Type II Toxin-Antitoxin Systems in Formation of *Escherichia coli* Type II Persister Cells. *mBio* 9(3).
11. Shan Y*, et al.* (2017) ATP-Dependent Persister Formation in *Escherichia coli*. *mBio* 8(1):e02267-02216.
12. Yamaoka Y (2010) Mechanisms of disease: *Helicobacter pylori* virulence factors. *Nat Rev Gastroenterol Hepatol* 7:629–641.

781 13. Amieva M & Peek Jr RM (2016) Pathobiology of *Helicobacter pylori*–Induced
782 Gastric Cancer. *Gastroenterology* 150(1):64-78.
783 14. Loke MF, Ng CG, Vilashni Y, Lim J, & Ho B (2016) Understanding the dimorphic
784 lifestyles of human gastric pathogen *Helicobacter pylori* using the SWATH-based
785 proteomics approach. *Scientific Reports* 6:26784.
786 15. Reshetnyak VI & Reshetnyak TM (2017) Significance of dormant forms of
787 *Helicobacter pylori* in ulcerogenesis. *World Journal of Gastroenterology*
788 23(27):4867-4878.
789 16. Ayrapetyan M, Williams T, & Oliver JD (2018) The relationship between the viable
790 but nonculturable state and antibiotic persister cells. *Journal of Bacteriology*.
791 17. Brantl S & Jahn N (2015) sRNAs in bacterial type I and type III toxin-antitoxin
792 systems. *FEMS Microbiol Rev.* 39:413-427.
793 18. Masachis S & Darfeuille F (2018) Type I Toxin-Antitoxin Systems: Regulating Toxin
794 Expression via Shine-Dalgarno Sequence Sequestration and Small RNA Binding.
795 *Microbiology Spectrum* 6(4).
796 19. Sharma CM, *et al.* (2010) The primary transcriptome of the major human pathogen
797 *Helicobacter pylori*. *Nature* 464:250-255.
798 20. Arnion H, *et al.* (2017) Mechanistic insights into type I toxin antitoxin systems in
799 *Helicobacter pylori*: the importance of mRNA folding in controlling toxin expression.
800 *Nucleic Acids Research* 45(8):4782-4795.
801 21. Boneca IG, *et al.* (2008) Development of inducible systems to engineer conditional
802 mutants of essential genes of *Helicobacter pylori*. *Appl. Environ. Microbiol.*
803 74(7):2095-2102.
804 22. Stingl K, Uhlemann E-M, Schmid R, Altendorf K, & Bakker EP (2002) Energetics of
805 *Helicobacter pylori* and Its Implications for the Mechanism of Urease-Dependent
806 Acid Tolerance at pH 1. *Journal of Bacteriology* 184(11):3053-3060.

807 23. Glauner B (1988) Separation and quantification of muropeptides with high-
808 performance liquid chromatography. *Anal Biochem.* 172:451-464.
809 24. Fischer F*, et al.* (2016) A novel essential ABC transporter and the NixA permease are
810 the two sole nickel uptake systems of *Helicobacter pylori*. *PLoS Pathog* 12:e1006018.
811 25. Brantl S (2012) Bacterial type I toxin-antitoxin systems. *RNA Biology* 9(12):1488-
812 1490.
813 26. Jahn N, Brantl S, & Strahl H (2015) Against the mainstream: the membrane‐
814 associated type I toxin BsrG from *Bacillus subtilis* interferes with cell envelope
815 biosynthesis without increasing membrane permeability. *Molecular Microbiology*
816 98(4):651-666.
817 27. Brielle R, Pinel-Marie M-L, & Felden B (2016) Linking bacterial type I toxins with
818 their actions. *Current Opinion in Microbiology* 30:114-121.
819 28. Unoson C & Wagner EGH (2008) A small SOS‐induced toxin is targeted against the
820 inner membrane in *Escherichia coli*. *Molecular Microbiology* 70(1):258-270.
821 29. Sayed N, Nonin-Lecomte S, Réty S, & Felden B (2012) Functional and Structural
822 Insights of a *Staphylococcus aureus* Apoptotic-like Membrane Peptide from a Toxin-
823 Antitoxin Module. *The Journal of Biological Chemistry* 287(52):43454-43463.
824 30. Kusters JG, Gerrits MM, Van Strijp JA, & Vandenbroucke-Grauls CM (1997)
825 Coccoid forms of *Helicobacter pylori* are the morphologic manifestation of cell death.
826 *Infection and Immunity* 65(9):3672-3679.
827 31. Enroth H*, et al.* (1999) In Vitro Aging of *Helicobacter pylori*: Changes in Morphology,
828 Intracellular Composition and Surface Properties. *Helicobacter* 4(1):7-16.
829 32. Costa K*, et al.* (1999) The Morphological Transition of *Helicobacter pylori* Cells from
830 Spiral to Coccoid Is Preceded by a Substantial Modification of the Cell Wall. *J.*
831 *Bacteriol* 181(12):3710-3715.

832 33. Yang DC, Blair KM, & Salama NR (2016) Staying in Shape: the Impact of Cell Shape
833 on Bacterial Survival in Diverse Environments. *Microbiology and Molecular Biology*
834 *Reviews : MMBR* 80(1):187-203.
835 34. Bonis M, Ecobichon C, Guadagnini S, Prévost M-C, & Boneca IG (2010) A M23B
836 family metallopeptidase of *Helicobacter pylori* required for cell shape, pole formation
837 and virulence. *Molecular Microbiology* 78(4):809-819.
838 35. Chaput C*, et al.* (2006) Role of AmiA in the Morphological Transition of
839 *Helicobacter pylori* and in Immune Escape. *PLoS Pathogens* 2(9):e97.
840 36. Heller DM, Tavag M, & Hochschild A (2017) CbtA toxin of *Escherichia coli* inhibits
841 cell division and cell elongation via direct and independent interactions with FtsZ and
842 MreB. *PLoS genetics* 13(9):e1007007.
843 37. Zeng H, Guo G, Mao XH, De Tong W, & Zou QM (2008) Proteomic Insights into
844 *Helicobacter pylori* Coccoid Forms Under Oxidative Stress. *Current Microbiology*
845 57(4):281.
846 38. Müller P*, et al.* (2016) A multistress responsive type I toxin-antitoxin system:
847 bsrE/SR5 from the *B. subtilis* chromosome. *RNA Biology* 13(5):511-523.
848 39. Cellini L (2014) *Helicobacter pylori*: A chameleon-like approach to life. *World*
849 *Journal of Gastroenterology* 20(19):5575-5582.
850 40. Segal ED, Falkow S, & Tompkins LS (1996) *Helicobacter pylori* attachment to gastric
851 cells induces cytoskeletal rearrangements and tyrosine phosphorylation of host cell
852 proteins. *Proceedings of the National Academy of Sciences of the United States of*
853 *America* 93(3):1259-1264.
854 41. Goldstein NS (2002) Chronic Inactive Gastritis and Coccoid *Helicobacter pylori* in
855 Patients Treated for Gastroesophageal Reflux Disease or With H pylori Eradication
856 Therapy. *American Journal of Clinical Pathology* 118(5):719-726.

857 42. Nagai S, *et al.* (2007) Role of Peyer's patches in the induction of *Helicobacter pylori*-
858 induced gastritis. *Proceedings of the National Academy of Sciences of the United*
859 *States of America* 104(21):8971-8976.
860 43. Cellini L, *et al.* (1994) Coccoid *Helicobacter pylori* not culturable *in vitro* reverts in
861 mice. *Microbiology and Immunology* 38(11):843-850.
862 44. Butcher LD, den Hartog G, Ernst PB, & Crowe SE (2017) Oxidative Stress Resulting
863 From *Helicobacter pylori* Infection Contributes to Gastric Carcinogenesis. *Cellular*
864 *and Molecular Gastroenterology and Hepatology* 3(3):316-322.
865 45. Ayrapetyan M, Williams TC, & Oliver JD (2015) Bridging the gap between viable but
866 non-culturable and antibiotic persistent bacteria. *Trends in microbiology* 23(1):7-13.
867 46. Rotem E, *et al.* (2010) Regulation of phenotypic variability by a threshold-based
868 mechanism underlies bacterial persistence. *Proceedings of the National Academy of*
869 *Sciences of the United States of America* 107(28):12541-12546.
870 47. Farnbacher M, *et al.* (2010) Sequencing, annotation and comparative genome analysis
871 of the gerbil-adapted *Helicobacter pylori* strain B8. *BMC Genom.* 11:335.: doi:
872 10.1186/1471-2164-1111-1335.
873 48. McClain MS, Shaffer CL, Israel DA, Peek RMJ, & Cover TL (2009) Genome
874 sequence analysis of *Helicobacter pylori* strains associated with gastric ulceration and
875 gastric cancer. *BMC Genom.* 10:3:doi: 10.1186/1471-2164-1110-1183.
876 49. Debowski AW, *et al.* (2012) Xer-cise in *Helicobacter pylori*: one-step transformation
877 for the construction of markerless gene deletions. *Helicobacter* 17:435-443.
878 50. Kutter S, *et al.* (2008) Protein Subassemblies of the *Helicobacter pylori* Cag Type IV
879 Secretion System Revealed by Localization and Interaction Studies. *Journal of*
880 *Bacteriology* 190(6):2161-2171.
881 51. El Ghachi M, *et al.* (2011) Characterization of the elongasome core PBP2: MreC
882 complex of *Helicobacter pylori*. *Molecular Microbiology* 82(1):68-86.

883 52. Muller C*, et al.* (2011) Hierarchical regulation of the NikR-mediated nickel response
884 in *Helicobacter pylori*. *Nucleic Acids Res.* 39:7564-7575.
885 53. Corbinais C, Mathieu A, Kortulewski T, Radicella JP, & Marsin S (2016) Following
886 transforming DNA in *Helicobacter pylori* from uptake to expression. *Mol Microbiol*
887 101(6):1039-1053.
888 54. Miller JH (1992) *A short Course in Bacterial Genetics : A laboratory manual and*
889 *handbook for Escherichia coli and related bacteria. Cold Spring Harbor, N. Y* (Cold
890 Spring Harbor Laboratory).

891

Figure 1

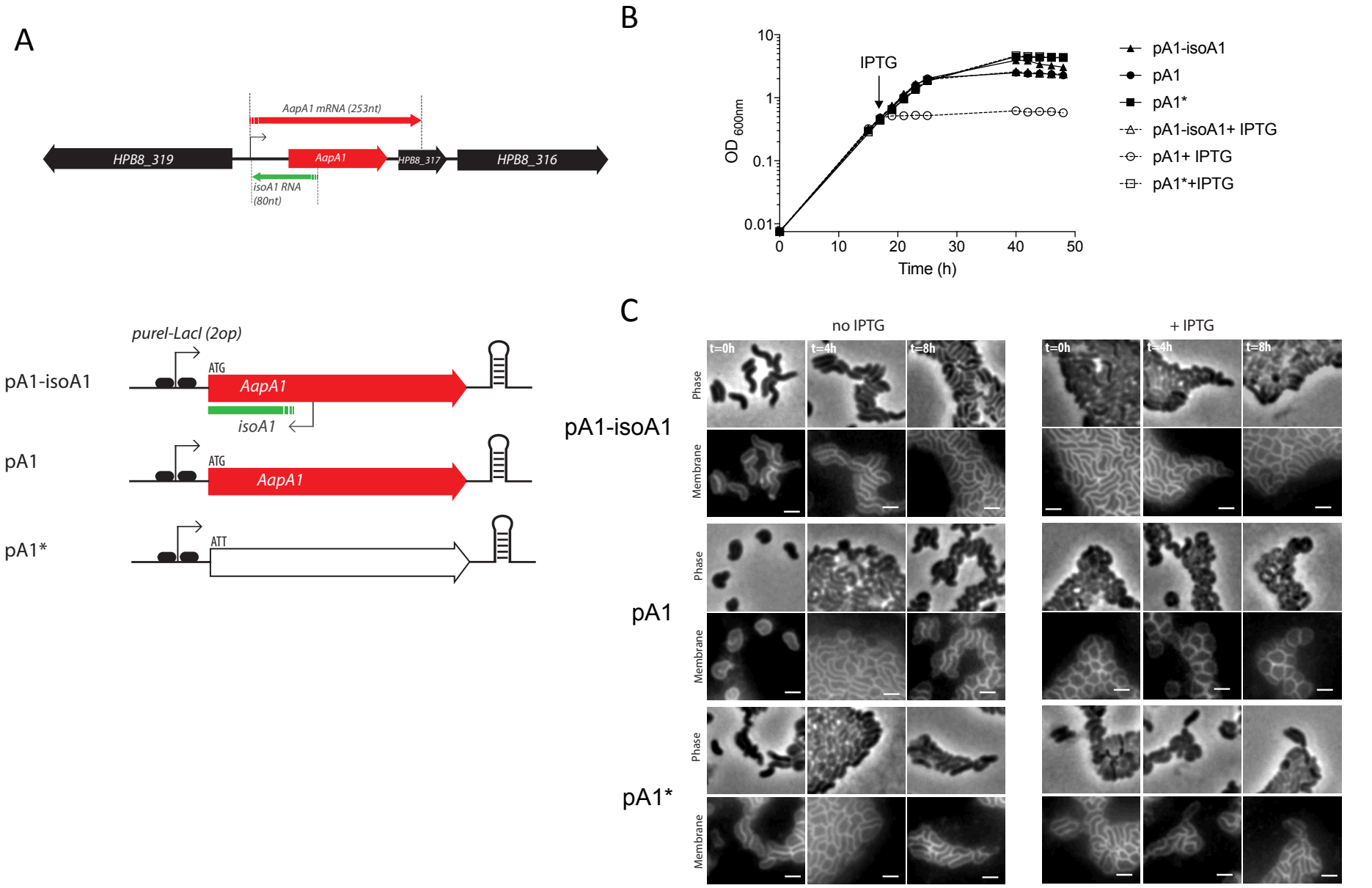
A
AapA1 mRNA (253nt)
HPB8_319
AapA1
HPB8_317
HPB8_316
isoA1 RNA (80nt)
purel-LacI (2op)
pA1-isoA1
ATG
AapA1
isoA1
pA1
ATG
AapA1
pA1*
ATT
B
IPTG
OD 600nm
10
1
0.1
0.01
0
10
20
30
40
50
Time (h)
pA1-isoA1
pA1
pA1*
pA1-isoA1+ IPTG
pA1+ IPTG
pA1*+IPTG
C
no IPTG
+ IPTG
t=0h
t=4h
t=8h
Phase
Membrane
pA1-isoA1
pA1
pA1*

Figure 2

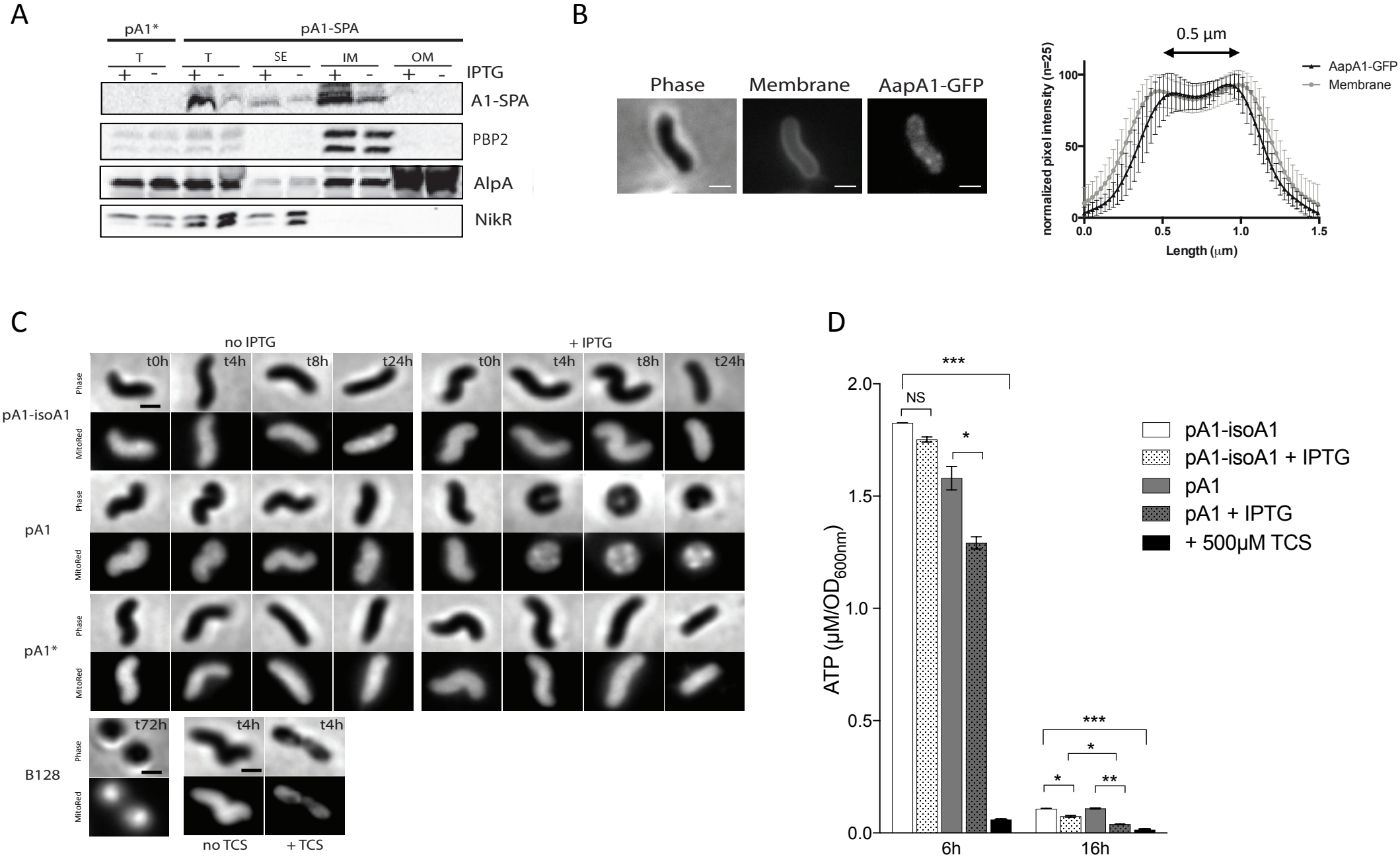
A
pA1*
pA1-SPA
T
T
SE
IM
OM
IPTG
A1-SPA
PBP2
AlpA
NikR
B
Phase
Membrane
AapA1-GFP
0.5 µm
AapA1-GFP
Membrane
normalized pixel intensity (n=25)
Length (µm)
C
no IPTG
+ IPTG
t0h
t4h
t8h
t24h
pA1-isoA1
pA1
pA1*
B128
Phase
MitoRed
t72h
no TCS
+ TCS
D
ATP (µM/OD600nm)
pA1-isoA1
pA1-isoA1 + IPTG
pA1
pA1 + IPTG
+ 500µM TCS
NS
6h
16h

Figure 3

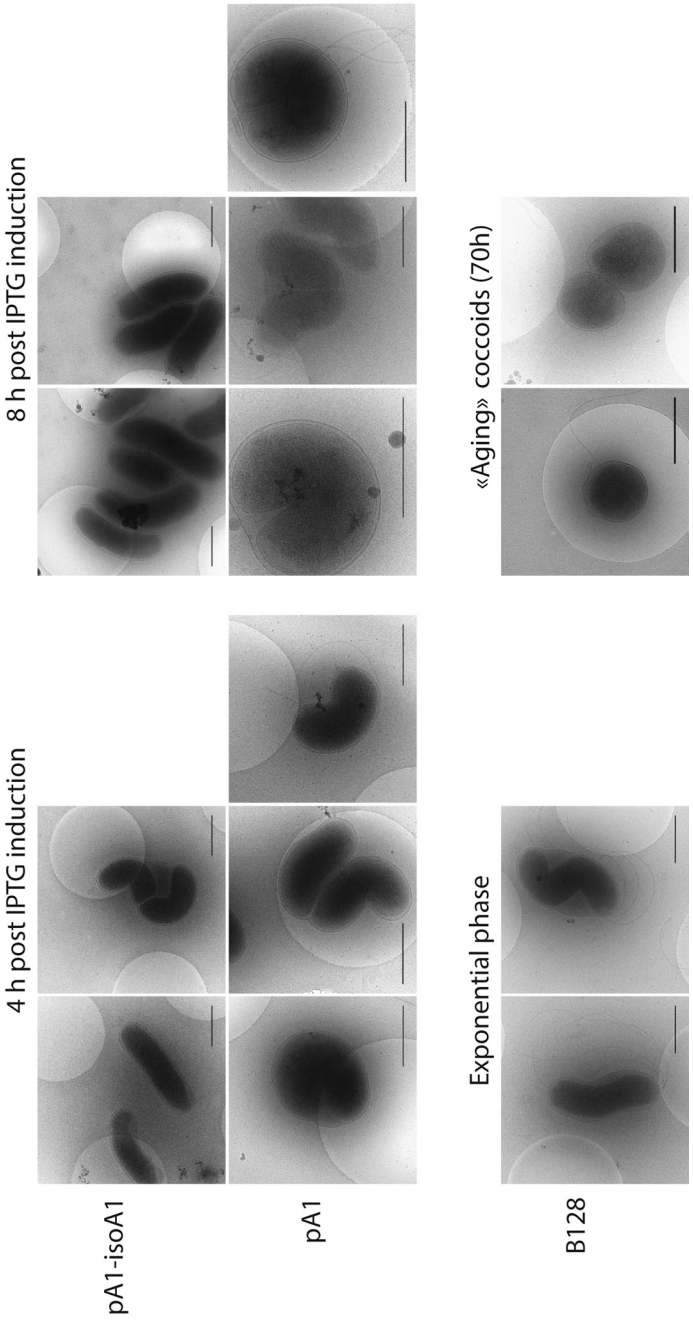

Figure 4

A

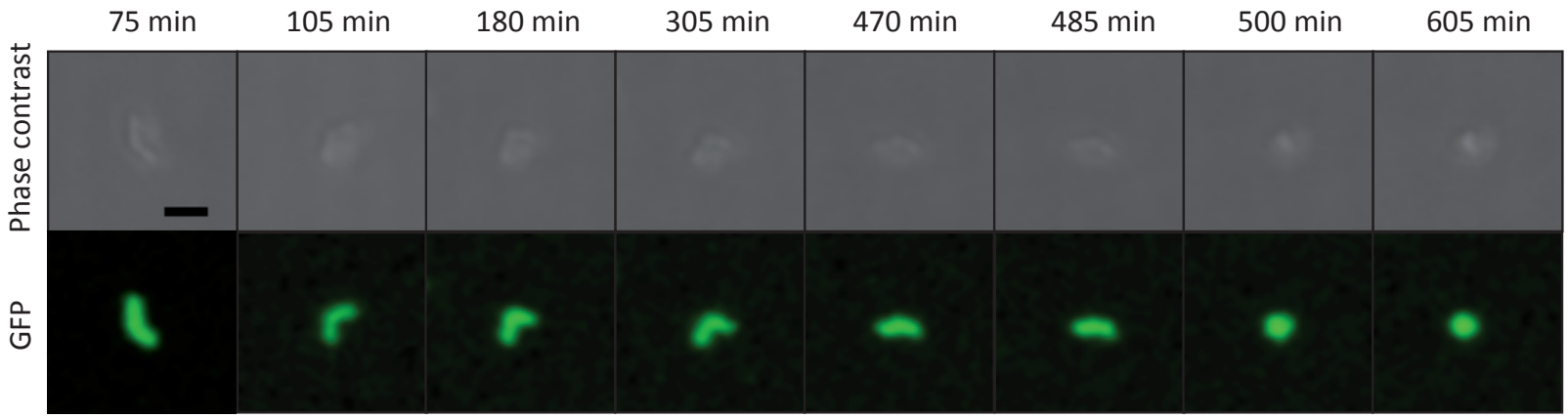

B

	Time before «bending» phenotype (min) 	Time before «pseudo-coccoid» phenotype (min) 	Time before «donut» phenotype (min) 	Maximum length before morphological change (µm)
Number of cells	49	37	21	63
Median	180	280	420	3.58
Mean ± SEM	185 ± 8.0	277 ± 16	420 ± 25.2	3.48 ± 0.08

Figure 5

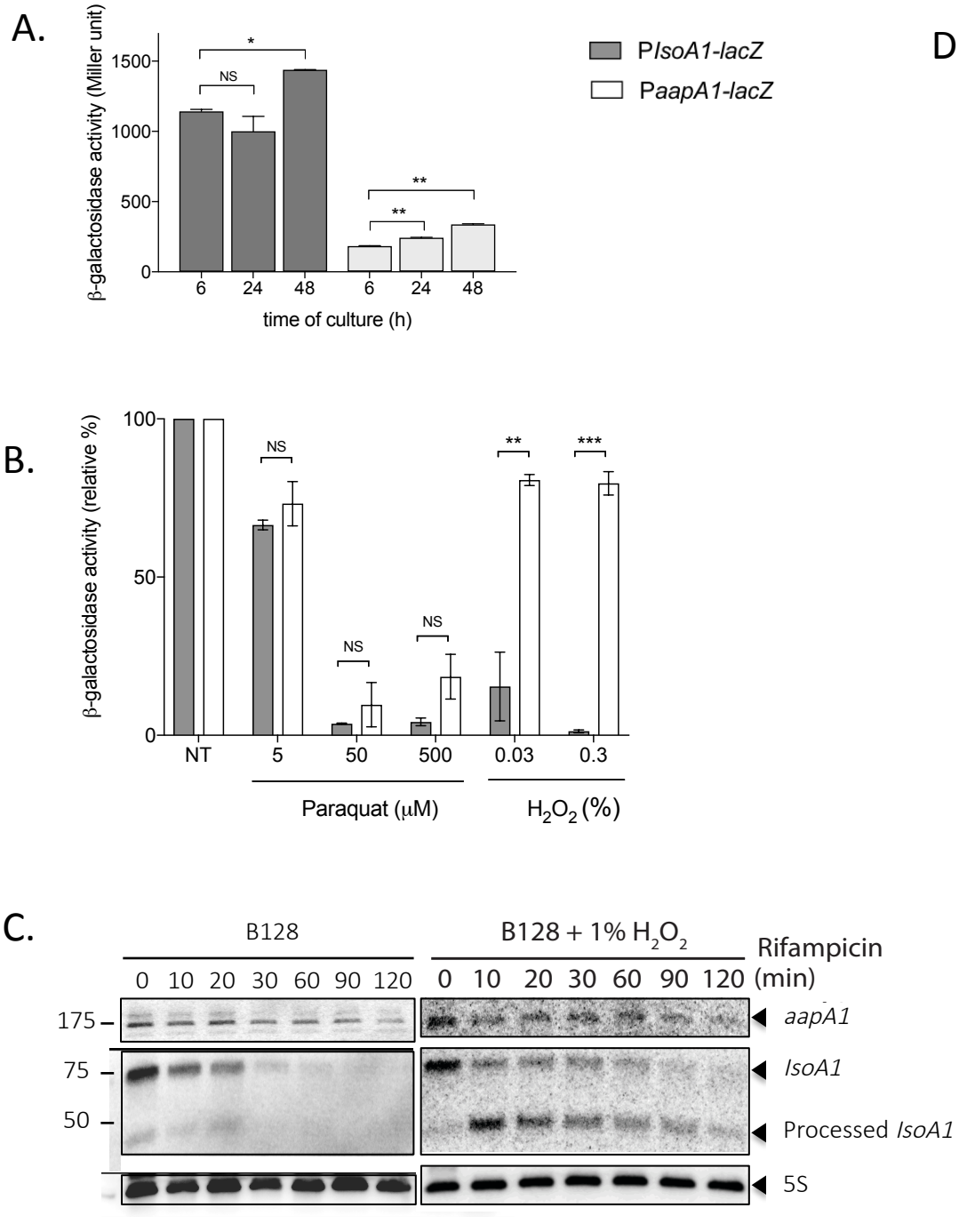
A.
β-galactosidase activity (Miller unit)
1500
1000
500
0
NS
*
**
**
6
24
48
6
24
48
time of culture (h)
PIsoA1-lacZ
PaapA1-lacZ
B.
β-galactosidase activity (relative %)
100
50
0
NS
NS
NS
**
***
NT
5
50
500
0.03
0.3
Paraquat (μM)
H2O2 (%)
C.
B128
B128 + 1% H2O2
Rifampicin
0 10 20 30 60 90 120
0 10 20 30 60 90 120
(min)
175
75
50
aapA1
IsoA1
Processed IsoA1
5S
D.
relative amounts of aapA1
1
0.1
0 20 40 60 80 100 120
time (min)
relative amounts of FL isoA1
1
0.1
0 20 40 60 80 100 120
time (min)
relative isoA1 (FL / processed)
1
0.1
0 20 40 60 80 100 120
time (min)
untreated
1% H2O2